

WUSH: Near-Optimal Adaptive Transforms for LLM Quantization

Jiale Chen

Institute of Science and Technology Austria (ISTA)

JIALE.CHEN@IST.AC.AT

Vage Egiazarian

Institute of Science and Technology Austria (ISTA)

VAGE.EGIAZARIAN@IST.AC.AT

Torsten Hoefler

ETH Zürich

TORSTEN.HOEFLER@INF.ETHZ.CH

Dan Alistarh

Institute of Science and Technology Austria (ISTA) & Red Hat AI

DAN.ALISTARH@IST.AC.AT

Abstract

Quantization to low bitwidth is a standard approach for deploying large language models, however, a few extreme weights and activations stretch the dynamic range and reduce the effective resolution of the quantizer. A common mitigation approach is to apply some fixed orthogonal transforms, such as Hadamard matrices, before quantization, which typically reduces the dynamic range. Yet, these transforms ignore the statistics of the data, and their optimality is currently not understood. In this work, we derive, for the first time, closed-form optimal linear blockwise transforms for joint weight-activation quantization using standard data-free quantizers for common numerical formats. Specifically, we provide derivations of the optimal *adaptive* (data-aware) transforms for round-to-nearest (RTN), AbsMax-scaled block quantizers for both integer and floating-point formats. The resulting construction, which we call WUSH, combines a Hadamard backbone with a data-dependent component based on second-order moments, yielding a non-orthogonal transform that is provably optimal under mild assumptions and remains structured for efficient implementation. Preliminary experimental results show that our approach consistently improves upon the Hadamard transform for common formats.

1 Introduction

1.1 Overview

Quantization of model weights (Dettmers et al., 2022; Frantar et al., 2023; Lin et al., 2024) or activations (Xiao et al., 2023; Ashkboos et al., 2024b) is now a standard tool for shrinking and accelerating large language models (LLMs) (Kurtic et al., 2025), making low-precision inference feasible on a wide range of hardware. A central difficulty, however, is that a few extreme “outlier” weights and activations expand the dynamic range and thereby degrade the effective resolution of low-bit representations.

It is known that one way to mitigate these outliers is to apply linear transforms before quantization (Jegou et al., 2008, 2010); in the case of LLM quantization, this is often in the form of rotations that spread variance more evenly across channels (Chee et al., 2023; Tseng et al., 2024a; Ashkboos et al., 2024b; Liu et al., 2025). For LLMs, Hadamard rotations have been remarkably effective, and blockwise variants aligned with quantization groups have also been shown to be useful in practice. The recent work of Egiazarian et al. (2025) shows that the block-wise Hadamard transform offers the best empirical performance for quantization among a large set of existing orthogonal transforms. Yet, these transforms are typically fixed and data-agnostic: in particular, the Hadamard transform does not depend on the statistics of the underlying weights or activations. This raises a natural question: if the Hadamard transform is *not data-aware*, in what sense can it be considered optimal for quantization?

In this work, we address this question by deriving *closed-form optimal linear blockwise transforms* for joint weight-activation quantization, which are generally *non-orthogonal* and *adaptive*, i.e., data-aware. As opposed to prior methods such as SpinQuant (Liu et al., 2025) or FlatQuant (Sun et al., 2024), our approach is closed-form and calibration-based, as it does not require training or fine-tuning.

We call our construction *WUSH*, and we show that it is optimal for floating-point (FP) block quantizers and asymptotically optimal for integer (INT) block quantizers. The name WUSH is a mnemonic for its composition. For a layer with *blockwise* weight $\mathbf{W}_{(i)}$ and calibration activation $\mathbf{X}_{(i)}$ in the i -th block, the WUSH transform $\mathbf{T}_{\text{hsuw}(i)}$ is constructed as

$$\mathbf{T}_{\text{hsuw}} = \mathbf{H} \mathbf{S}_{(i)}^{-\frac{1}{2}} \mathbf{U}_{(i)}^\top \mathbf{W}_{(i)}'^\top \quad (1)$$

where $\mathbf{W}_{(i)}'$ is the Cholesky decomposition of $\mathbf{W}_{(i)} \mathbf{W}_{(i)}^\top = \mathbf{W}_{(i)}' \mathbf{W}_{(i)}'^\top$, the matrices $\mathbf{U}_{(i)}$, $\mathbf{S}_{(i)}$, $\mathbf{V}_{(i)}$ are from the singular value decomposition (SVD) of $\mathbf{W}_{(i)}'^\top \mathbf{X}_{(i)} = \mathbf{U}_{(i)} \mathbf{S}_{(i)} \mathbf{V}_{(i)}^\top$, and \mathbf{H} is a Hadamard matrix. We will define it again in a more exhaustive manner in Eq. (6). WUSH is explicitly adapted to minimize loss in second-order statistics while retaining a structure amenable to efficient implementation and providing a principled, data-aware alternative to heuristic Hadamard-style and blockwise rotations.

1.2 Related Work

Post-training quantization and outliers. Generic post-training quantization schemes, such as RTN (round-to-nearest), OBQ (Frantar & Alistarh, 2022), and GPTQ (Frantar et al., 2023), are highly sensitive to heavy-tailed outliers in the weights and activations of LLMs because a small number of extreme values determine the quantization scale. As a result, most quantization levels are spent covering rare extremes instead of the bulk of the distribution, which leads to a significant loss of accuracy.

Non-uniform bitwidths and explicit outlier storage. One common strategy to mitigate outliers is to use non-uniform bitwidths. Methods such as LLM.int8() (Dettmers et al., 2022), SpQR (Dettmers et al., 2024), and QUIK (Ashkboos et al., 2024a) explicitly separate and store outliers in higher precision, while HPTQ (Chen et al., 2025) uses Huffman encoding to compress the outliers and reduce their storage costs. These approaches can achieve high

accuracy at a low effective bitwidth, however, the resulting formats are irregular and require specialized kernels and additional engineering effort for efficient deployment.

Transform-based outlier mitigation. Another line of work applies transforms to the weights and activations before quantization to reduce the impact of outliers. SmoothQuant (Xiao et al., 2023) and AWQ (Lin et al., 2024) rescale channels to stabilize the dynamic ranges of weights and activations. QuIP (Chee et al., 2023) introduces an incoherence processing step. QuIP# (Tseng et al., 2024a), QTIP (Tseng et al., 2024b), and QuaRot (Ashkboos et al., 2024b) use Hadamard transforms to spread outlier energy across channel dimensions, while SpinQuant (Liu et al., 2025) learns rotations optimized on calibration data. However, their transforms are either heuristic, costly to learn, or primarily designed for weight-only quantization, which limits their accuracy or practicality when applied to fast, per-token activation quantization in large models.

Blockwise transforms and emerging FP formats. The recent FP formats, such as MXFP (MX Alliance, 2023) and NVFP (NVIDIA, 2024), have motivated blockwise transform schemes. Shao et al. (2025) indicates that blockwise Hadamard transforms can be more effective under these FP formats than full-layer transforms, but Egiazarian et al. (2025) highlights the limited gains achievable with Hadamard alone, linking this to the properties of the underlying weight and activation distributions. In contrast, our work derives a closed-form, data-aware optimal blockwise transform (WUSH) and analyzes how such a transform interacts with both FP and INT block quantizers.

1.3 Methodology

Problem setup. We formulate the transformed weight-activation quantization problem as follows. Define $\mathbf{W} \in \mathbb{R}^{d_{\text{in}} \times d_{\text{out}}}$ as the weight of a linear layer with d_{in} input channels and d_{out} output channels. Define $\mathbf{X} \in \mathbb{R}^{d_{\text{in}} \times d_{\text{batch}}}$ as the calibration input activation with d_{in} embedding channels and d_{batch} tokens. Define $q(\cdot)$ as a quantizer that maps a matrix of continuous values to quantized values (we will specify q later). Let $\mathbf{T}_{\mathbf{W}}, \mathbf{T}_{\mathbf{X}} \in \mathbb{R}^{d_{\text{in}} \times d_{\text{in}}}$ be the transforms applied to \mathbf{W} and \mathbf{X} , respectively. For weight-activation quantization, the output activation $\mathbf{W}^\top \mathbf{X}$ becomes $q(\mathbf{T}_{\mathbf{W}} \mathbf{W})^\top q(\mathbf{T}_{\mathbf{X}} \mathbf{X})$. Our goal is to choose $\mathbf{T}_{\mathbf{W}}, \mathbf{T}_{\mathbf{X}}$ such that the L_2 output loss

$$\ell = d_{\text{out}}^{-1} d_{\text{batch}}^{-1} \left\| q(\mathbf{T}_{\mathbf{W}} \mathbf{W})^\top q(\mathbf{T}_{\mathbf{X}} \mathbf{X}) - \mathbf{W}^\top \mathbf{X} \right\|_{\text{F}}^2 \quad (2)$$

is minimized under the given quantizer q . The constant $d_{\text{out}}^{-1} d_{\text{batch}}^{-1}$ is added to simplify the analysis later.

Block-independent constraint. While the weights can be pre-quantized, the activations must be transformed and quantized *dynamically* at inference time. To reduce the computational overhead and simplify the problem, we constrain the transforms $\mathbf{T}_{\mathbf{W}}$ and $\mathbf{T}_{\mathbf{X}}$ to be block-diagonal, and the quantizer q to be an RTN (round-to-nearest) quantizer with AbsMax (the maximum absolute value within a group) scales. We assume that the quantization is applied to each sub-column vector of shape $d \times 1$ and that the transform block size aligns

with the quantization group size d (d is a factor of d_{in} , and d is a power of 2). Denote

$$\mathbf{T}_W = \text{diag}(\mathbf{T}_{W_{(1)}}, \dots, \mathbf{T}_{W_{(d_{\text{in}}/d)}}) \quad \text{and} \quad \mathbf{T}_X = \text{diag}(\mathbf{T}_{X_{(1)}}, \dots, \mathbf{T}_{X_{(d_{\text{in}}/d)}}) \quad (3)$$

with $\mathbf{T}_{W_{(i)}}, \mathbf{T}_{X_{(i)}} \in \mathbb{R}^{d \times d}$. We partition $\mathbf{W}^\top = [\mathbf{W}_{(1)}^\top, \dots, \mathbf{W}_{(d_{\text{in}}/d)}^\top]$ with $\mathbf{W}_{(i)} \in \mathbb{R}^{d \times d_{\text{out}}}$ and $\mathbf{X}^\top = [\mathbf{X}_{(1)}^\top, \dots, \mathbf{X}_{(d_{\text{in}}/d)}^\top]$ with $\mathbf{X}_{(i)} \in \mathbb{R}^{d \times d_{\text{batch}}}$. Then, we can express the output without quantization as $\mathbf{W}^\top \mathbf{X} = \sum_{i=1}^{d_{\text{in}}/d} \mathbf{W}_{(i)}^\top \mathbf{X}_{(i)}$ and the output with weight-activation quantization as

$$q(\mathbf{T}_W \mathbf{W})^\top q(\mathbf{T}_X \mathbf{X}) = \sum_{i=1}^{d_{\text{in}}/d} q(\mathbf{T}_{W_{(i)}} \mathbf{W}_{(i)})^\top q(\mathbf{T}_{X_{(i)}} \mathbf{X}_{(i)}). \quad (4)$$

Finally, define the blockwise output loss as

$$\ell_{(i)} = d_{\text{out}}^{-1} d_{\text{batch}}^{-1} \left\| q(\mathbf{T}_{W_{(i)}} \mathbf{W}_{(i)})^\top q(\mathbf{T}_{X_{(i)}} \mathbf{X}_{(i)}) - \mathbf{W}_{(i)}^\top \mathbf{X}_{(i)} \right\|_F^2. \quad (5)$$

We approximate the layerwise loss as $\ell \approx \sum_{i=1}^{d_{\text{in}}/d} \ell_{(i)}$ and minimize the blockwise loss $\ell_{(i)}$ independently.

Optimal block-diagonal transforms. We will prove that there exist closed-form optimal transforms for each block under reasonable assumptions and smooth approximations, which are optimal for FP and asymptotically optimal for INT quantizations. Let $\mathbf{W}'_{(i)}, \mathbf{X}'_{(i)} \in \mathbb{R}^{d \times d}$ be matrices that satisfy $\mathbf{W}'_{(i)} \mathbf{W}_{(i)}^\top = d_{\text{out}}^{-1} \mathbf{W}_{(i)} \mathbf{W}_{(i)}^\top$ and $\mathbf{X}'_{(i)} \mathbf{X}_{(i)}^\top = d_{\text{batch}}^{-1} \mathbf{X}_{(i)} \mathbf{X}_{(i)}^\top$, respectively. Without loss of generality (any differences will be canceled in later steps), we let \mathbf{W}' and \mathbf{X}' be the lower triangular matrices from the Cholesky decomposition of the second moments $d_{\text{out}}^{-1} \mathbf{W}_{(i)} \mathbf{W}_{(i)}^\top$ and $d_{\text{batch}}^{-1} \mathbf{X}_{(i)} \mathbf{X}_{(i)}^\top$. In the case of $\text{rank}(\mathbf{W}_{(i)}) < d$ or $\text{rank}(\mathbf{X}_{(i)}) < d$, we can dampen the diagonal of the second moment before the Cholesky decomposition. Let the orthogonal matrices $\mathbf{U}_{(i)}, \mathbf{V}_{(i)} \in \mathbb{R}^{d \times d}$ and the diagonal matrix $\mathbf{S}_{(i)} \in \mathbb{R}^{d \times d}$ be the singular value decomposition (SVD) of $\mathbf{W}'_{(i)} \mathbf{X}'_{(i)} = \mathbf{U}_{(i)} \mathbf{S}_{(i)} \mathbf{V}_{(i)}^\top$. Let $\mathbf{H} \in \mathbb{R}^{d \times d}$ be a normalized (orthogonal) Hadamard matrix where each element is $\pm d^{-\frac{1}{2}}$. The optimal $\mathbf{T}_{W_{(i)}}$ and $\mathbf{T}_{X_{(i)}}$ are constructed as

$$\mathbf{T}_{\text{hsvx}(i)} = \mathbf{H} \mathbf{S}_{(i)}^{-\frac{1}{2}} \mathbf{V}_{(i)}^\top \mathbf{X}'_{(i)}^\top \quad \text{and} \quad \mathbf{T}_{\text{hsuw}(i)} = \mathbf{H} \mathbf{S}_{(i)}^{-\frac{1}{2}} \mathbf{U}_{(i)}^\top \mathbf{W}'_{(i)}^\top, \quad (6)$$

respectively. Note that $\mathbf{T}_{\text{hsvx}(i)} = \mathbf{T}_{\text{hsuw}(i)}^{-\top}$ ¹, which can be easily verified by calculating $\mathbf{T}_{\text{hsvx}(i)} \mathbf{T}_{\text{hsuw}(i)}^\top = \mathbf{I}$ with \mathbf{I} as the identity matrix.

Remark. The Hadamard matrix \mathbf{H} is the only data-agnostic ingredient in our optimal formulation in Eq. (6), which explains why it has been empirically shown to be one of the most effective data-agnostic orthogonal transforms.

1. The $-\top$ superscript notation means $(\cdot)^{-\top} = ((\cdot)^{-1})^\top = ((\cdot)^\top)^{-1}$.

2 Theoretical Derivation

In this section, we focus on the question of finding optimal transforms that minimize the loss of one block $\ell_{(i)}$. We omit the subscript (i) to simplify notation.

2.1 Problem Setup and General Proof Approach

Probabilistic reformulation. We reformulate the problem from a probabilistic perspective. We split the matrices $\mathbf{W} = [\mathbf{w}_1, \dots, \mathbf{w}_{d_{\text{out}}}]$ and $\mathbf{X} = [\mathbf{x}_1, \dots, \mathbf{x}_{d_{\text{batch}}}]$ into columns $\mathbf{w}_k, \mathbf{x}_k \in \mathbb{R}^d$ and treat the columns as i.i.d. samples from d -dimensional independent distributions $\mathbf{w} \sim \mathcal{D}_{\mathbf{w}}$ and $\mathbf{x} \sim \mathcal{D}_{\mathbf{x}}$, respectively. Then the matrices \mathbf{W}' and \mathbf{X}' satisfy $\mathbf{W}'\mathbf{W}'^\top = \mathbb{E}_{\mathbf{w}}\mathbf{w}\mathbf{w}^\top$ and $\mathbf{X}'\mathbf{X}'^\top = \mathbb{E}_{\mathbf{x}}\mathbf{x}\mathbf{x}^\top$, respectively. We can reinterpret the blockwise loss as $\ell = \mathbb{E}_{\mathbf{w}, \mathbf{x}} \left(q(\mathbf{T}_{\mathbf{W}}\mathbf{w})^\top q(\mathbf{T}_{\mathbf{X}}\mathbf{x}) - \mathbf{w}^\top \mathbf{x} \right)^2$.

Unbiased quantization. We assume that q is a stochastic and unbiased quantizer, i.e., for a vector $\boldsymbol{\alpha} \in \mathbb{R}^d$, the quantization error $\varepsilon(\boldsymbol{\alpha}) = q(\boldsymbol{\alpha}) - \boldsymbol{\alpha}$ is a random vector with $\mathbb{E}_{\varepsilon(\boldsymbol{\alpha})}\varepsilon(\boldsymbol{\alpha}) = \mathbf{0}$. We further constrain $\mathbf{T}_{\mathbf{W}} = \mathbf{T}_{\mathbf{X}}^{-\top}$ such that $q(\mathbf{T}_{\mathbf{W}}\mathbf{w})^\top q(\mathbf{T}_{\mathbf{X}}\mathbf{x})$ is unbiased with respect to $\mathbf{w}^\top \mathbf{x}$. Then, using the first-order approximation, we can split ℓ into two non-negative terms:

$$\begin{aligned} \ell &= \mathbb{E}_{\mathbf{w}, \mathbf{x}, \varepsilon(\mathbf{T}_{\mathbf{W}}\mathbf{w}), \varepsilon(\mathbf{T}_{\mathbf{X}}\mathbf{x})} \left((\mathbf{T}_{\mathbf{W}}\mathbf{w} + \varepsilon(\mathbf{T}_{\mathbf{W}}\mathbf{w}))^\top (\mathbf{T}_{\mathbf{X}}\mathbf{x} + \varepsilon(\mathbf{T}_{\mathbf{X}}\mathbf{x})) - \mathbf{w}^\top \mathbf{x} \right)^2 \\ &= \mathbb{E}_{\mathbf{w}, \mathbf{x}, \varepsilon(\mathbf{T}_{\mathbf{W}}\mathbf{w}), \varepsilon(\mathbf{T}_{\mathbf{X}}\mathbf{x})} \left(\mathbf{x}^\top \mathbf{T}_{\mathbf{X}}^\top \varepsilon(\mathbf{T}_{\mathbf{W}}\mathbf{w}) + \mathbf{w}^\top \mathbf{T}_{\mathbf{W}}^\top \varepsilon(\mathbf{T}_{\mathbf{X}}\mathbf{x}) + \varepsilon(\mathbf{T}_{\mathbf{W}}\mathbf{w})^\top \varepsilon(\mathbf{T}_{\mathbf{X}}\mathbf{x}) \right)^2 \\ &\approx \mathbb{E}_{\mathbf{w}, \mathbf{x}, \varepsilon(\mathbf{T}_{\mathbf{W}}\mathbf{w}), \varepsilon(\mathbf{T}_{\mathbf{X}}\mathbf{x})} \left(\mathbf{x}^\top \mathbf{T}_{\mathbf{X}}^\top \varepsilon(\mathbf{T}_{\mathbf{W}}\mathbf{w}) + \mathbf{w}^\top \mathbf{T}_{\mathbf{W}}^\top \varepsilon(\mathbf{T}_{\mathbf{X}}\mathbf{x}) \right)^2 \\ &= \left(\mathbb{E}_{\mathbf{w}, \varepsilon(\mathbf{T}_{\mathbf{W}}\mathbf{w})} \left\| \mathbf{X}'^\top \mathbf{T}_{\mathbf{X}}^\top \varepsilon(\mathbf{T}_{\mathbf{W}}\mathbf{w}) \right\|^2 \right) + \left(\mathbb{E}_{\mathbf{x}, \varepsilon(\mathbf{T}_{\mathbf{X}}\mathbf{x})} \left\| \mathbf{W}'^\top \mathbf{T}_{\mathbf{W}}^\top \varepsilon(\mathbf{T}_{\mathbf{X}}\mathbf{x}) \right\|^2 \right) \\ &= \left(\mathbb{E}_{\mathbf{w}, \varepsilon(\mathbf{T}_{\mathbf{W}}\mathbf{w})} \left\| \mathbf{X}'^\top \mathbf{T}_{\mathbf{W}}^{-1} \varepsilon(\mathbf{T}_{\mathbf{W}}\mathbf{w}) \right\|^2 \right) + \left(\mathbb{E}_{\mathbf{x}, \varepsilon(\mathbf{T}_{\mathbf{X}}\mathbf{x})} \left\| \mathbf{W}'^\top \mathbf{T}_{\mathbf{X}}^{-1} \varepsilon(\mathbf{T}_{\mathbf{X}}\mathbf{x}) \right\|^2 \right). \end{aligned} \tag{7}$$

Problem reduction. We can compute the optimal $\mathbf{T}_{\mathbf{W}}$ and $\mathbf{T}_{\mathbf{X}}$ individually for each of the non-negative terms and verify if $\mathbf{T}_{\mathbf{W}} = \mathbf{T}_{\mathbf{X}}^{-\top}$. The two terms have similar forms and can be optimized in similar ways. We focus on finding the optimal $\mathbf{T}_{\mathbf{X}}$ for the second term. Define the d -dimensional random variable $\mathbf{y} = \mathbf{W}'^\top \mathbf{x} \sim \mathcal{D}_{\mathbf{y}}$. Define the transformation matrix $\mathbf{T} = \mathbf{T}_{\mathbf{X}}\mathbf{W}'^{-\top}$. Then, the second term becomes

$$\begin{aligned} \mathbb{E}_{\mathbf{x}, \varepsilon(\mathbf{T}_{\mathbf{X}}\mathbf{x})} \left\| \mathbf{W}'^\top \mathbf{T}_{\mathbf{X}}^{-1} \varepsilon(\mathbf{T}_{\mathbf{X}}\mathbf{x}) \right\|^2 &= \mathbb{E}_{\mathbf{x}, \varepsilon(\mathbf{T}_{\mathbf{X}}\mathbf{x})} \left\| \left(\mathbf{T}_{\mathbf{X}}\mathbf{W}'^{-\top} \right)^{-1} \varepsilon \left(\mathbf{T}_{\mathbf{X}} \left(\mathbf{W}'^{-\top} \mathbf{x} \right) \right) \right\|^2 \\ &= \mathbb{E}_{\mathbf{y}, \varepsilon(\mathbf{T}\mathbf{y})} \left\| \mathbf{T}^{-1} \varepsilon(\mathbf{T}\mathbf{y}) \right\|^2 \end{aligned} \tag{8}$$

Therefore, the two-sided quantization problem is reduced to finding the optimal $\mathbf{T} \in \mathbb{R}^{d \times d}$ that minimizes the one-sided quantization loss $\mathbb{E}_{\mathbf{y}, \varepsilon(\mathbf{T}\mathbf{y})} \left\| \mathbf{T}^{-1} \varepsilon(\mathbf{T}\mathbf{y}) \right\|^2$ and compute $\mathbf{T}_{\mathbf{X}} = \mathbf{T}\mathbf{W}'^\top$.

Transformation parameterization. Let the unknown orthogonal matrices $\mathbf{U}', \mathbf{R} \in \mathbb{R}^{d \times d}$ and the unknown diagonal matrix $\mathbf{S}' \in \mathbb{R}^{d \times d}$ be the singular value decomposition (SVD)

of $TUS = U'S'R^\top$; thus, T can be parameterized as $T = U'S'R^\top S^{-1}U^\top$. Denote $S = \text{diag}(s_1, \dots, s_d)$ and $S' = \text{diag}(s'_1, \dots, s'_d)$. Without loss of generality, assume $s_1 \geq \dots \geq s_d > 0$ and $s'_1 \geq \dots \geq s'_d > 0$.

Theorem 1 (Optimal Transform) *The optimal configuration of T for floating-point (FP) data types is $U' = H$, $S' = S^{\frac{1}{2}}$, and $R = I$. For integer (INT), the same configuration is optimal up to a $d^{o(1)}$ factor for zero-mean Gaussian/Laplacian distributed data and within a d factor for any distribution.*

Proof We provide detailed proofs for FP and INT in Sections 2.2 and 2.3, respectively. For each data type, we apply a two-step proof strategy. We first provide a smooth modeling of the quantizer and treat the type casting errors as random noise. Secondly, we calculate the expected quantization error with respect to the parameterized transform and minimize this expectation by solving the corresponding optimization problem. ■

Some useful notations and basic results are as follows:

- Denote the k -th standard basis vector as $\mathbf{e}_k \in \{0, 1\}^d$, where the k -th element is 1 and 0 otherwise.
- The second moment of \mathbf{y} is $\mathbb{E}_{\mathbf{y}} \mathbf{y} \mathbf{y}^\top = \mathbf{W}'^\top (\mathbb{E}_{\mathbf{x}} \mathbf{x} \mathbf{x}^\top) \mathbf{W}' = \mathbf{W}'^\top \mathbf{X}' \mathbf{X}'^\top \mathbf{W}' = \mathbf{U} \mathbf{S}^2 \mathbf{U}^\top$.
- The second moment of $T\mathbf{y}$ is $\mathbb{E}_{\mathbf{y}} T\mathbf{y} (T\mathbf{y})^\top = T (\mathbb{E}_{\mathbf{y}} \mathbf{y} \mathbf{y}^\top) T^\top = \mathbf{U}' \mathbf{S}'^2 \mathbf{U}'^\top$.
- The expected squared norm of \mathbf{y} is $\mathbb{E}_{\mathbf{y}} \|\mathbf{y}\|^2 = \text{tr}(\mathbb{E}_{\mathbf{y}} \mathbf{y} \mathbf{y}^\top) = \text{tr}(\mathbf{U} \mathbf{S}^2 \mathbf{U}^\top) = \text{tr}(\mathbf{S}^2)$.
- Similarly, the expected squared norm of $T\mathbf{y}$ is $\mathbb{E}_{\mathbf{y}} \|T\mathbf{y}\|^2 = \text{tr}(\mathbf{S}'^2)$.
- Because $\mathbf{S} \succ \mathbf{0}$, $(\text{tr}(\mathbf{S}))^2 \geq \text{tr}(\mathbf{S}^2)$. By Jensen's inequality, $\text{tr}(\mathbf{S}^2) \geq d^{-1} (\text{tr}(\mathbf{S}))^2$.

2.2 Proof for Floating-Point (FP) Types

2.2.1 QUANTIZATION ERROR MODELING

Theorem 2 (FP Quantization Error Modeling) *For a vector $\boldsymbol{\alpha} \in \mathbb{R}^d$, we can model the quantization error $\varepsilon(\boldsymbol{\alpha}) = \text{diag}(\boldsymbol{\eta}) \boldsymbol{\alpha}$ with $\boldsymbol{\eta} = [\eta_1, \dots, \eta_d]^\top \in \mathbb{R}^d$ being a random vector of i.i.d. samples $\eta \sim \mathcal{D}_\eta$ and $\mathbb{E}_\eta \eta = 0$.*

Proof The FP format EaMb is defined as a tuple (s, e, m) with a sign $s \in \{0, 1\}$, an exponent $e \in \{0, \dots, 2^a - 1\}$, and a mantissa $m \in \{0, \dots, 2^b - 1\}$. Assume we do not need to consider the subnormal and special number cases. The tuple (s, e, m) represents the number $x_{\text{EaMb}} = (-1)^s 2^{e-2^{a-1}+1} (1 + 2^{-b}m)$.

Using the approximation $1 + (\cdot) \approx 2^{(\cdot)}$ for $2^{-b}m \in [0, 1]$, we define a smoothed version of EaMb, named SEaMb, as $x_{\text{SEaMb}} = (-1)^s 2^{e-2^{a-1}+1} 2^{2^{-b}m} = (-1)^s 2^{2^{-b}(2^b e + m) - 2^{a-1}+1}$ with $2^b e + m = 2^b (\log_2 |x_{\text{SEaMb}}| + 2^{a-1} - 1)$ being a $a + b$ bit unsigned integer (concatenating the

binary representations of e and m). The minimum of $|x_{\text{SEaMb}}|$ is $\min |x_{\text{SEaMb}}| = 2^{-2^{a-1}+1}$ and the maximum is $\max |x_{\text{SEaMb}}| = 2^{2^{-b}(2^{a+b}-1)-2^{a-1}+1} = 2^{2^{a-1}-2^{-b}+1}$.

Denote $\text{SEaMb}(x)$ as the quantizer that casts $x \in [-\max |x_{\text{SEaMb}}|, \max |x_{\text{SEaMb}}|]$ to the nearest number in the SEaMb type. Assume $e \in (-\infty, 2^a - 1]$ so that the smaller values can be represented more precisely. $\text{SEaMb}(x)$ can be approximated using integer rounding in the logarithm space and first-order expansion. For $x \neq 0$,

$$\begin{aligned} \text{SEaMb}(x) &\approx \text{sgn}(x) 2^{2^{-b} \lfloor 2^b (\log_2 |x| + 2^{a-1} - 1) \rfloor - 2^{a-1} + 1} = \text{sgn}(x) 2^{2^{-b} \lfloor 2^b \log_2 |x| \rfloor} \\ &\approx \text{sgn}(x) \left(2^{2^{-b} 2^b \log_2 |x|} + \left(\lfloor 2^b \log_2 |x| \rfloor - 2^b \log_2 |x| \right) 2^{2^{-b} 2^b \log_2 |x|} 2^{-b \ln 2} \right) \quad (9) \\ &= x \left(1 + \left(\lfloor 2^b \log_2 |x| \rfloor - 2^b \log_2 |x| \right) 2^{-b \ln 2} \right). \end{aligned}$$

For $x = 0$, $\text{SEaMb}(0) \approx \lim_{x \rightarrow 0} x \left(1 + (\lfloor 2^b \log_2 |x| \rfloor - 2^b \log_2 |x|) 2^{-b \ln 2} \right) = 0$. We model the casting error $\text{SEaMb}(x) - x = (\ln 2) 2^{-b} \xi x$ where $x \in [-\max |x_{\text{SEaMb}}|, \max |x_{\text{SEaMb}}|]$ and the random variable $\xi \sim \text{Uniform}(-2^{-1}, 2^{-1})$.

For a quantization format that uses EaMb for values and $\text{E}\tilde{\text{aMb}}$ for scales, we approximate it with a scalar quantizer $q(x) = \text{SEaMb}(xs^{-1}) \text{SE}\tilde{\text{aMb}}(s)$ where $x \in \mathbb{R}$, scale $s \in \mathbb{R}_{\neq 0}$, $|s| \leq \max |x_{\text{SE}\tilde{\text{aMb}}}|$, and $|xs^{-1}| \leq \max |x_{\text{SEaMb}}|$. Then,

$$\begin{aligned} q(x) &= \text{SEaMb}(xs^{-1}) \text{SE}\tilde{\text{aMb}}(s) = \left(1 + (\ln 2) 2^{-b} \xi \right) xs^{-1} \left(1 + (\ln 2) 2^{-\tilde{b}} \tilde{\xi} \right) s \\ &= \left(1 + (\ln 2) 2^{-b} \xi \right) \left(1 + (\ln 2) 2^{-\tilde{b}} \tilde{\xi} \right) x \end{aligned} \quad (10)$$

with the independent random variables $\xi, \tilde{\xi} \sim \text{Uniform}(-2^{-1}, 2^{-1})$.

Define $\eta = \left(1 + (\ln 2) 2^{-b} \xi \right) \left(1 + (\ln 2) 2^{-\tilde{b}} \tilde{\xi} \right) - 1$. The quantization error is $q(x) - x = \eta x$.

$$\mathbb{E}_\eta \eta = \mathbb{E}_{\xi, \tilde{\xi}} (\ln 2) 2^{-b} \xi + (\ln 2) 2^{-\tilde{b}} \tilde{\xi} + (\ln 2)^2 2^{-b-\tilde{b}} \xi \tilde{\xi} = 0. \quad (11)$$

■

2.2.2 LOSS MINIMIZATION

Using Theorem 2, the minimization objective is

$$\begin{aligned} \mathbb{E}_{\mathbf{y}, \varepsilon(\mathbf{T}\mathbf{y})} \left\| \mathbf{T}^{-1} \varepsilon(\mathbf{T}\mathbf{y}) \right\|^2 &= \mathbb{E}_{\mathbf{y}, \boldsymbol{\eta}} \left\| \mathbf{T}^{-1} \text{diag}(\boldsymbol{\eta}) \mathbf{T}\mathbf{y} \right\|^2 \\ &= \mathbb{E}_{\mathbf{y}, \boldsymbol{\eta}} \text{tr} \left(\mathbf{y}^\top \mathbf{T}^\top \text{diag}(\boldsymbol{\eta}) \mathbf{T}^{-\top} \mathbf{T}^{-1} \text{diag}(\boldsymbol{\eta}) \mathbf{T}\mathbf{y} \right) \\ &= \mathbb{E}_{\mathbf{y}, \boldsymbol{\eta}} \text{tr} \left(\mathbf{T}^{-1} \text{diag}(\boldsymbol{\eta}) \mathbf{T}\mathbf{y}\mathbf{y}^\top \mathbf{T}^\top \text{diag}(\boldsymbol{\eta}) \mathbf{T}^{-\top} \right) \quad (12) \\ &= \text{tr} \left(\mathbf{T}^{-1} \left(\mathbb{E}_{\boldsymbol{\eta}} \text{diag}(\boldsymbol{\eta}) \mathbf{T} \left(\mathbb{E}_{\mathbf{y}} \mathbf{y}\mathbf{y}^\top \right) \mathbf{T}^\top \text{diag}(\boldsymbol{\eta}) \right) \mathbf{T}^{-\top} \right) \\ &= (\mathbb{E}_{\boldsymbol{\eta}} \boldsymbol{\eta}^2) \text{tr} \left(\mathbf{T}^{-1} \left(\left(\mathbf{U}' \mathbf{S}'^2 \mathbf{U}'^\top \right) \odot \mathbf{I} \right) \mathbf{T}^{-\top} \right) \end{aligned}$$

where \odot represents elementwise multiplication. The lower bound of the trace term in the loss is

$$\begin{aligned}
& \text{tr} \left(\mathbf{T}^{-1} \left(\left(\mathbf{U}' \mathbf{S}'^2 \mathbf{U}'^\top \right) \odot \mathbf{I} \right) \mathbf{T}^{-\top} \right) \\
&= \text{tr} \left(\mathbf{T}^{-1} \text{diag} \left(\left\| \mathbf{S}' \mathbf{U}'^\top \mathbf{e}_1 \right\|^2, \dots, \left\| \mathbf{S}' \mathbf{U}'^\top \mathbf{e}_d \right\|^2 \right) \mathbf{T}^{-\top} \right) \\
&= \sum_{j=1}^d \sum_{k=1}^d (\mathbf{e}_j^\top \mathbf{T}^{-1} \mathbf{e}_k)^2 \left\| \mathbf{S}' \mathbf{U}'^\top \mathbf{e}_k \right\|^2 \\
&= \sum_{k=1}^d \left\| \mathbf{T}^{-1} \mathbf{e}_k \right\|^2 \left\| \mathbf{S}' \mathbf{U}'^\top \mathbf{e}_k \right\|^2 \\
&= \sum_{k=1}^d \left\| \mathbf{U} \mathbf{S} \mathbf{R} \mathbf{S}'^{-1} \mathbf{U}'^\top \mathbf{e}_k \right\|^2 \left\| \mathbf{S}' \mathbf{U}'^\top \mathbf{e}_k \right\|^2 \\
&= \sum_{k=1}^d \left\| \mathbf{S} \mathbf{R} \mathbf{S}'^{-1} \mathbf{U}'^\top \mathbf{e}_k \right\|^2 \left\| \mathbf{R} \mathbf{S}' \mathbf{U}'^\top \mathbf{e}_k \right\|^2 \quad (\text{rotation-invariance of } L_2 \text{ norm}) \\
&\geq \sum_{k=1}^d \left(\mathbf{e}_k^\top \mathbf{U}' \mathbf{S}'^{-1} \mathbf{R}^\top \mathbf{S} \mathbf{R} \mathbf{S}' \mathbf{U}'^\top \mathbf{e}_k \right)^2 \quad (\text{Cauchy-Schwarz}) \\
&= d \left(d^{-1} \sum_{k=1}^d \left(\mathbf{e}_k^\top \mathbf{U}' \mathbf{S}'^{-1} \mathbf{R}^\top \mathbf{S} \mathbf{R} \mathbf{S}' \mathbf{U}'^\top \mathbf{e}_k \right)^2 \right) \\
&\geq d \left(d^{-1} \sum_{k=1}^d \mathbf{e}_k^\top \mathbf{U}' \mathbf{S}'^{-1} \mathbf{R}^\top \mathbf{S} \mathbf{R} \mathbf{S}' \mathbf{U}'^\top \mathbf{e}_k \right)^2 \quad (\text{Jensen}) \\
&= d^{-1} \left(\text{tr} \left(\mathbf{U}' \mathbf{S}'^{-1} \mathbf{R}^\top \mathbf{S} \mathbf{R} \mathbf{S}' \mathbf{U}'^\top \right) \right)^2 \\
&= d^{-1} (\text{tr}(\mathbf{S}))^2.
\end{aligned} \tag{13}$$

The equality can be attained by choosing $\mathbf{U}' = \mathbf{H}$, $\mathbf{S}' = \mathbf{S}^{\frac{1}{2}}$, and $\mathbf{R} = \mathbf{I}$ such that

$$\begin{aligned}
& \text{tr} \left(\mathbf{T}^{-1} \left(\left(\mathbf{U}' \mathbf{S}'^2 \mathbf{U}'^\top \right) \odot \mathbf{I} \right) \mathbf{T}^{-\top} \right) = \sum_{k=1}^d \left\| \mathbf{S} \mathbf{R} \mathbf{S}'^{-1} \mathbf{U}'^\top \mathbf{e}_k \right\|^2 \left\| \mathbf{R} \mathbf{S}' \mathbf{U}'^\top \mathbf{e}_k \right\|^2 \\
&= \sum_{k=1}^d \left(\left\| \mathbf{S}^{\frac{1}{2}} \mathbf{H}^\top \mathbf{e}_k \right\|^2 \right)^2 = \sum_{k=1}^d \left(\sum_{j=1}^d s_j \left(\mathbf{e}_j^\top \mathbf{H}^\top \mathbf{e}_k \right)^2 \right)^2 = \sum_{k=1}^d \left(\sum_{j=1}^d s_j d^{-1} \right)^2 \quad (14) \\
&= d^{-1} (\text{tr}(\mathbf{S}))^2.
\end{aligned}$$

2.2.3 DISCUSSION

Under our smooth modeling in Theorem 2, for any orthogonal \mathbf{T} (including the identity $\mathbf{T} = \mathbf{I}$ and the Hadamard $\mathbf{T} = \mathbf{H}$), the minimization objective

$$\begin{aligned} \mathbb{E}_{\mathbf{y}, \varepsilon(\mathbf{T}\mathbf{y})} \|\mathbf{T}^{-1} \varepsilon(\mathbf{T}\mathbf{y})\|^2 &= \mathbb{E}_{\mathbf{y}, \boldsymbol{\eta}} \|\mathbf{T}^{-1} \text{diag}(\boldsymbol{\eta}) \mathbf{T}\mathbf{y}\|^2 = \mathbb{E}_{\mathbf{y}} \mathbf{y}^\top \mathbf{T}^\top \left(\mathbb{E}_{\boldsymbol{\eta}} \text{diag}(\boldsymbol{\eta})^2 \right) \mathbf{T}\mathbf{y} \\ &= (\mathbb{E}_{\boldsymbol{\eta}} \boldsymbol{\eta}^2) \mathbb{E}_{\mathbf{y}} \|\mathbf{y}\|^2 = (\mathbb{E}_{\boldsymbol{\eta}} \boldsymbol{\eta}^2) \text{tr}(\mathbf{S}^2) \geq (\mathbb{E}_{\boldsymbol{\eta}} \boldsymbol{\eta}^2) d^{-1} (\text{tr}(\mathbf{S}))^2 \geq (\mathbb{E}_{\boldsymbol{\eta}} \boldsymbol{\eta}^2) d^{-1} \text{tr}(\mathbf{S}^2), \end{aligned} \quad (15)$$

so the orthogonal transforms will not be helpful for reducing the quantization error. Also note that the non-trivial choices $\mathbf{U}' = \mathbf{H}$ and $\mathbf{S}' = \mathbf{S}^{\frac{1}{2}}$ are both essential for reducing the error by at most d times, with $\text{tr}(\mathbf{S}) \approx s_1$ being the extreme case scenario. Either trivial choices of $\mathbf{U}' = \mathbf{I}$ or $\mathbf{S}' = \mathbf{I}$ will lead to the same suboptimal trace term $\text{tr}(\mathbf{T}^{-1} ((\mathbf{U}' \mathbf{S}'^2 \mathbf{U}'^\top) \odot \mathbf{I}) \mathbf{T}^{-\top}) = \text{tr}(\mathbf{S}^2)$, which is the same as the case of orthogonal \mathbf{T} .

2.3 Proof for Integer (INT) Data Types

2.3.1 QUANTIZATION ERROR MODELING

We model the quantization error using pseudo noise similar to DiffQ (Défossez et al., 2022).

Theorem 3 (INT Quantization Error Modeling) *For a vector $\boldsymbol{\alpha} \in \mathbb{R}^d$, we can model the quantization error $\varepsilon(\boldsymbol{\alpha}) = \|\boldsymbol{\alpha}\|_\infty \boldsymbol{\eta}$ with $\boldsymbol{\eta} = [\eta_1, \dots, \eta_d]^\top \in \mathbb{R}^d$ being a random vector of i.i.d. samples $\eta \sim \mathcal{D}_\eta$ and $\mathbb{E}_\eta \boldsymbol{\eta} = 0$.*

Proof Define the scalar quantizer of b -bit symmetric integer as $q(x) = (\lfloor xs^{-1} \rfloor + 2^{-1})s$, where $x \in \mathbb{R}$, scale $s \in \mathbb{R}_{\neq 0}$, and $xs^{-1} \in [-2^{b-1}, 2^{b-1})$. To simplify the analysis, we model the quantizer as $q(x) = (xs^{-1} + \xi)s = x + s\xi$ with random noise $\xi \sim \text{Uniform}(-2^{-1}, 2^{-1})$. For a vector $\boldsymbol{\alpha} \in \mathbb{R}^d$, we use the AbsMax scale $s = 2^{1-b} \|\boldsymbol{\alpha}\|_\infty$. Define $\eta = 2^{1-b}\xi$, then we have $s\xi = \eta \|\boldsymbol{\alpha}\|_\infty$. The quantization error $\varepsilon(\boldsymbol{\alpha}) = \|\boldsymbol{\alpha}\|_\infty \boldsymbol{\eta}$ with $\boldsymbol{\eta} = [\eta_1, \dots, \eta_d]^\top \in \mathbb{R}^d$ being a random vector of i.i.d. samples $\eta \sim \mathcal{D}_\eta$ and $\mathbb{E}_\eta \boldsymbol{\eta} = 2^{1-b} \mathbb{E}_\xi \xi = 0$. ■

2.3.2 LOSS MINIMIZATION

Using Theorem 3, the minimization objective is

$$\begin{aligned} \mathbb{E}_{\mathbf{y}, \varepsilon(\mathbf{T}\mathbf{y})} \|\mathbf{T}^{-1} \varepsilon(\mathbf{T}\mathbf{y})\|^2 &= \mathbb{E}_{\mathbf{y}, \boldsymbol{\eta}} \|\mathbf{T}^{-1} \|\mathbf{T}\mathbf{y}\|_\infty \boldsymbol{\eta}\|^2 \\ &= \text{tr} \left(\mathbf{T}^{-1} (\mathbb{E}_{\boldsymbol{\eta}} \boldsymbol{\eta} \boldsymbol{\eta}^\top) \mathbf{T}^{-\top} \right) \mathbb{E}_{\mathbf{y}} \|\mathbf{T}\mathbf{y}\|_\infty^2 = (\mathbb{E}_{\boldsymbol{\eta}} \boldsymbol{\eta}^2) \text{tr}(\mathbf{T}^{-1} \mathbf{T}^{-\top}) \mathbb{E}_{\mathbf{y}} \|\mathbf{T}\mathbf{y}\|_\infty^2 \\ &= (\mathbb{E}_{\boldsymbol{\eta}} \boldsymbol{\eta}^2) \|\mathbf{T}^{-1}\|_{\text{F}}^2 \mathbb{E}_{\mathbf{y}} \|\mathbf{T}\mathbf{y}\|_\infty^2. \end{aligned} \quad (16)$$

We can obtain a lower bound for the term $\|\mathbf{T}^{-1}\|_{\text{F}}^2 = \text{tr}(\mathbf{T}^{-1} \mathbf{T}^{-\top}) = \text{tr}(\mathbf{U} \mathbf{S} \mathbf{R} \mathbf{S}'^{-2} \mathbf{R}^\top \mathbf{S} \mathbf{U}^\top) = \text{tr}(\mathbf{S}^2 \mathbf{R} \mathbf{S}'^{-2} \mathbf{R}^\top)$. Because $s_1^2 \geq \dots \geq s_d^2$ and $s_1'^{-2} \leq \dots \leq s_d'^{-2}$, using von Neumann's trace

inequality, we obtain:

$$\|T^{-1}\|_F^2 = \text{tr} \left(S^2 R S'^{-2} R^\top \right) \geq \text{tr} (S^2 S'^{-2}). \quad (17)$$

Equality is attained when $R = I$.

Next, we obtain the lower and upper bounds for the term $\mathbb{E}_y \|Ty\|_\infty^2$. Express the expectations as $\mathbb{E}_y \|Ty\|_\infty^2 = \mathbb{E}_y \max_k (\mathbf{e}_k^\top Ty)^2 \geq \max_k \mathbb{E}_y (\mathbf{e}_k^\top Ty)^2$ (Jensen's inequality) and $\mathbb{E}_y \|Ty\|^2 = \mathbb{E}_y \sum_{k=1}^d (\mathbf{e}_k^\top Ty)^2 = \sum_{k=1}^d \mathbb{E}_y (\mathbf{e}_k^\top Ty)^2$. By the relationships among the mean, maximum, and summation values, we have:

$$d^{-1} \mathbb{E}_y \|Ty\|^2 \leq \max_k \mathbb{E}_y (\mathbf{e}_k^\top Ty)^2 \leq \mathbb{E}_y \|Ty\|_\infty^2 \leq \mathbb{E}_y \|Ty\|^2 \leq d \max_k \mathbb{E}_y (\mathbf{e}_k^\top Ty)^2, \quad (18)$$

where $\mathbb{E}_y \|Ty\|^2 = \text{tr} (S'^2)$ and $\mathbb{E}_y (\mathbf{e}_k^\top Ty)^2 = \mathbf{e}_k^\top T (\mathbb{E}_y yy^\top) T^\top \mathbf{e}_k = \mathbf{e}_k^\top U' S'^2 U'^\top \mathbf{e}_k = \|S' U'^\top \mathbf{e}_k\|^2$.

Lemma 4 (Maximum Inequalities for Tail-Bounded Distributions) *If $X_1, \dots, X_d \in \mathbb{R}$ are zero-mean Gaussian random variables,*

$$\mathbb{E} \max_k X_k^2 \leq \min \{d, (2 \ln(2d) + 2)\} \max_k \mathbb{E} X_k^2. \quad (19)$$

If $X_1, \dots, X_d \in \mathbb{R}$ are zero-mean Laplacian random variables,

$$\mathbb{E} \max_k X_k^2 \leq \left(2^{-1} (\ln d)^2 + \ln d + 1\right) \max_k \mathbb{E} X_k^2. \quad (20)$$

Both inequalities hold without the need for independence.

Proof We provide proofs for Gaussian and Laplacian distributions in Sections A.1 and A.2, respectively. ■

Using Lemma 4, for a tail-bounded \mathcal{D}_y that is a zero-mean multivariate Gaussian or Laplacian, we can further tighten the upper bound by

$$\mathbb{E}_y \|Ty\|_\infty^2 \leq \min \left\{ d^{o(1)} \max_k \mathbb{E}_y (\mathbf{e}_k^\top Ty)^2, \mathbb{E}_y \|Ty\|^2 \right\}. \quad (21)$$

When $U' = H$, the marginal second moment becomes $\mathbb{E}_y (\mathbf{e}_k^\top Ty)^2 = \|S' U'^\top \mathbf{e}_k\|^2 = \|S' H^\top \mathbf{e}_k\|^2 = \sum_{j=1}^d s_j'^2 d^{-1} = d^{-1} \text{tr} (S'^2) = d^{-1} \mathbb{E}_y \|Ty\|^2$, which is equalized for all k , and $\max_k \mathbb{E}_y (\mathbf{e}_k^\top Ty)^2$ is minimized to $d^{-1} \mathbb{E}_y \|Ty\|^2$. Taken together, by setting $R = I$ and $U' = H$, the term $\|T^{-1}\|_F^2 \mathbb{E}_y \|Ty\|_\infty^2$ is bounded by $\text{tr} (S^2 S'^{-2}) \text{tr} (S'^2)$ within a gap of d such that

$$d^{-1} \text{tr} (S^2 S'^{-2}) \text{tr} (S'^2) \leq \|T^{-1}\|_F^2 \mathbb{E}_y \|Ty\|_\infty^2 \leq \text{tr} (S^2 S'^{-2}) \text{tr} (S'^2). \quad (22)$$

And for a tail-bounded \mathcal{D}_y , the gap is narrowed to $d^{o(1)}$ such that

$$\|T^{-1}\|_F^2 \mathbb{E}_y \|Ty\|_\infty^2 = d^{o(1)-1} \text{tr} (S^2 S'^{-2}) \text{tr} (S'^2). \quad (23)$$

By the Cauchy-Schwarz inequality,

$$\text{tr}(\mathbf{S}^2 \mathbf{S}'^{-2}) \text{tr}(\mathbf{S}'^2) \geq \left(\text{tr} \left((\mathbf{S}^2 \mathbf{S}'^{-2})^{\frac{1}{2}} (\mathbf{S}'^2)^{\frac{1}{2}} \right) \right)^2 = (\text{tr}(\mathbf{S}))^2 \quad (24)$$

and the equality is attained when $\mathbf{S}' \propto \mathbf{S}^{\frac{1}{2}}$. Without loss of generality, we can choose $\mathbf{S}' = \mathbf{S}^{\frac{1}{2}}$ to minimize both the lower and upper bounds of the quantization loss.

2.3.3 DISCUSSION

Consider the case of \mathbf{T} being orthogonal. $\|\mathbf{T}^{-1}\|_{\text{F}}^2 = d$ and $\mathbb{E}_{\mathbf{y}} \|\mathbf{T}\mathbf{y}\|^2 = \mathbb{E}_{\mathbf{y}} \|\mathbf{y}\|^2 = \text{tr}(\mathbf{S}^2)$. For any distribution $\mathcal{D}_{\mathbf{y}}$, the bounds are $\text{tr}(\mathbf{S}^2) \leq \|\mathbf{T}^{-1}\|_{\text{F}}^2 \mathbb{E}_{\mathbf{y}} \|\mathbf{T}\mathbf{y}\|_{\infty}^2 \leq d \text{tr}(\mathbf{S}^2)$. For the Hadamard $\mathbf{T} = \mathbf{H}$ and a tail-bounded $\mathcal{D}_{\mathbf{y}}$, $\|\mathbf{T}^{-1}\|_{\text{F}}^2 \mathbb{E}_{\mathbf{y}} \|\mathbf{T}\mathbf{y}\|_{\infty}^2 = d^{o(1)} \text{tr}(\mathbf{S}^2)$ with high probability. Because $\text{tr}(\mathbf{S}^2) \geq d^{-1} (\text{tr}(\mathbf{S}))^2 \geq d^{-1} \text{tr}(\mathbf{S}^2)$, an orthogonal \mathbf{T} is suboptimal, and the error bounds of an orthogonal \mathbf{T} can be at most d times larger than those of the optimal \mathbf{T} , with $\text{tr}(\mathbf{S}) \approx s_1$ being the extreme case scenario.

3 Experiments

3.1 Algorithm

Algorithm 1: Compute WUSH Transforms and Pre-Quantize Weights

Input: weights $\mathbf{W} \in \mathbb{R}^{d_{\text{in}} \times d_{\text{out}}}$, activations $\mathbf{X} \in \mathbb{R}^{d_{\text{in}} \times d_{\text{batch}}}$, damping ratio $\lambda \in \mathbb{R}$

Output: WUSH transform $\mathbf{T}_{\text{hsuw}(i)} \in \mathbb{R}^{d \times d}$ and pre-quantized weight

$\hat{\mathbf{W}}_{(i)} \in \mathbb{R}^{d \times d_{\text{out}}}$ for each block $i = 1, \dots, d_{\text{in}}/d$

```

1  $\mathcal{M}_{\mathbf{X}} \leftarrow d_{\text{batch}}^{-1} \mathbf{X} \mathbf{X}^{\top} + \lambda \mathbf{I}$  // same as GPTQ's Hessian
2  $\mathcal{M}_{\mathbf{W}} \leftarrow d_{\text{out}}^{-1} \mathbf{W} \mathbf{W}^{\top} + \lambda \mathbf{I}$ 
3 for  $i \leftarrow 1$  to  $d_{\text{in}}/d$  (in parallel) do
4    $j_1, j_2 \leftarrow (i-1)d + 1, id$ 
5    $\mathbf{M}_{\mathbf{X}} \leftarrow \mathcal{M}_{\mathbf{X}}[j_1 : j_2, j_1 : j_2]$  // select the block with row/column index from  $j_1$ 
    (inclusive) to  $j_2$  (inclusive)
6    $\mathbf{M}_{\mathbf{W}} \leftarrow \mathcal{M}_{\mathbf{W}}[j_1 : j_2, j_1 : j_2]$  // select the block with row/column index from
     $j_1$  (inclusive) to  $j_2$  (inclusive)
7    $\mathbf{W}' \leftarrow \text{Cholesky}(\mathbf{M}_{\mathbf{W}})$  //  $\mathbf{W}' \mathbf{W}'^{\top} = \mathbf{M}_{\mathbf{W}}$ 
8    $\mathbf{U}, \mathbf{\Lambda} \leftarrow \text{Eigendecomposition}(\mathbf{W}'^{\top} \mathbf{M}_{\mathbf{X}} \mathbf{W}')$  //  $\mathbf{U} \mathbf{\Lambda} \mathbf{U}^{\top} = \mathbf{W}'^{\top} \mathbf{M}_{\mathbf{X}} \mathbf{W}'$ 
9    $\mathbf{T}_{\text{hsuw}(i)} \leftarrow \mathbf{H} \mathbf{\Lambda}^{-\frac{1}{4}} \mathbf{U}^{\top} \mathbf{W}'^{\top}$  // WUSH transform
10   $\hat{\mathbf{W}}_{(i)} = q \left( \mathbf{T}_{\text{hsuw}(i)}^{-\top} \mathbf{W}[j_1 : j_2, 1 : d_{\text{out}}] \right)$  // pre-quantize weight block
11 end
```

Algorithm 1 summarizes the procedure used to compute the blockwise transforms and pre-quantized weights for each linear layer. In practice, the required second-order information can be obtained either from the calibration activations or from the Hessian matrix; the

latter coincides, up to a constant factor, with the Hessian used in GPTQ. As a result, the calibration pipeline closely follows that of GPTQ: layers are processed sequentially, and after processing a layer, the calibration activations are propagated through the quantized layer to provide the inputs for calibrating the next one.

During inference, the forward pass is calculated as

$$\sum_{i=1}^{d_{\text{in}}/d} \hat{\mathbf{W}}_{(i)}^{\top} q\left(\mathbf{T}_{\text{hsuw}(i)} \mathbf{X}_{(i)}\right). \quad (25)$$

with the symbol \mathbf{X} being overloaded as the new activations instead of the calibration ones.

3.2 Layer Loss

Table 1: Weight-activation RTN quantization losses with identity (I), random rotation (R), Hadamard (H), WUSH without Hadamard (WUS), and WUSH transforms.

Format	Transform	Q	K	V	O	Gate	Up	Down
MXFP4	I	.01105	.01201	.01068	.00435	.00710	.00656	.00547
	R	.00761	.00773	.00914	.00384	.00556	.00568	.00407
	H	.00724	.00720	.00860	.00379	.00545	.00561	.00390
	WUS	.00627	.00722	.00405	.00357	.00576	.00475	.00446
	WUSH	.00334	.00334	.00330	.00276	.00449	.00439	.00339
NVFP4	I	.00423	.00435	.00437	.00234	.00349	.00341	.00241
	R	.00498	.00501	.00586	.00254	.00363	.00368	.00266
	H	.00560	.00562	.00670	.00258	.00371	.00379	.00278
	WUS	.00226	.00236	.00230	.00200	.00304	.00301	.00223
	WUSH	.00240	.00244	.00228	.00192	.00309	.00302	.00233
INT4	I	.17004	.12277	.01315	.00455	.05585	.00983	.01934
	R	.00579	.00584	.00696	.00294	.00422	.00429	.00310
	H	.00557	.00555	.00680	.00286	.00409	.00425	.00303
	WUS	.21268	.14233	.01067	.00454	.05021	.00742	.01308
	WUSH	.00239	.00243	.00254	.00210	.00343	.00343	.00255

We report the layerwise weight-activation RTN quantization loss (L_2 loss normalized by the number of elements) for each linear layer in the 18th transformer block of Qwen3-8B, using 32 calibration samples of sequence length 2048 from the FineWeb-Edu (Penedo et al., 2024) dataset. We compare the WUSH transform with the identity (I), random rotation (R) averaged over 10 runs, Hadamard (H), and WUSH without Hadamard (WUS). Table 1 summarizes the losses for MXFP4, NVFP4, and INT4 formats, where INT4 denotes 4-bit integers with Gaussian MSE clipping and BF16 scales of group size 32. Across formats, WUSH substantially reduces the loss: WUSH consistently yields the smallest loss for MXFP4 and INT4, while WUSH and WUS are almost equally optimal for NVFP4.

These empirical trends are broadly consistent with our theoretical analysis, suggesting that the approximation assumptions (Section 2.1) and the smooth error models (Sections 2.2.1 and 2.3.1) capture the dominant sources of quantization loss in practice. At the same time, MXFP4 behaves as a hybrid between ideal FP and INT quantization: the effective mantissa step changes uniformly, imparting INT-like behavior, especially in the subnormal regime and small exponent ranges. This helps explain why Hadamard transforms still provide measurable gains for the MXFP4 format, despite the ideal FP theory (Section 2.2.3) predicting no benefit for purely orthogonal transforms.

3.3 LLM Benchmarks

We now present preliminary experiments evaluating the accuracy of models using the WUSH transform, relative to the identity (standard RTN) and Hadamard. We conduct our experiment on the LLama-3.2-3B-Instruct, LLama3.1-8B-Instruct, Qwen3-8B, and Qwen3-14B models. We use Platinumbench (Vendrow et al., 2025) and the LM Eval Harness (Gao et al., 2021) for evaluation.

The full results for LM Eval Harness tasks are shown in Table 2. Here, we observe that WUSH achieves the highest average recovery score among all the methods tested, often by large margins. Remarkably, on large models such as Qwen3-14B, it helps narrow the accuracy gap between MXFP4 and NVFP4 to nearly 0.5%.

We plot the results for Platinumbench in Figures 1 to 4. Again, we observe that WUSH provides significant accuracy improvements, especially in the case of MXFP4.

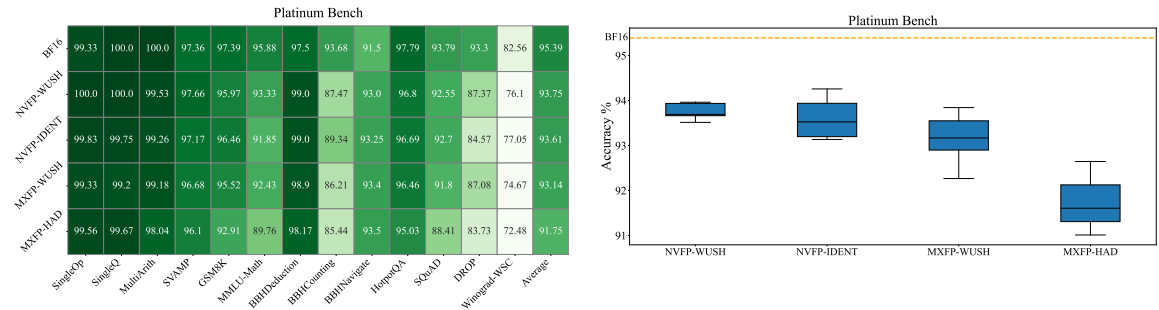


Figure 1: Comparison of different transforms on Qwen3-8B for both NVFP4 and MXFP4 RTN quantization on Platinum benchmark tasks. The left table shows accuracy results across the individual Platinum benchmark tasks, while the right plot shows the average accuracy scores together with their standard deviations for each transform.

4 Future Work

A natural next step is to integrate WUSH with advanced post-training quantization schemes such as GPTQ. In this setting, the weights are updated iteratively through error propagation, while WUSH is constructed from the second-order statistics of the updated weights. Designing an algorithm that jointly updates the weights and the associated blockwise transforms is

Table 2: Accuracy results on the LM Eval Harness for round-to-nearest (RTN) quantization of weights and activations with identity (I), Hadamard (H), and WUSH transforms.

Model	Format	Transform	MMLU	GSM8K	HellaSwag	WinoGrande	Avg.	Recovery%
Llama-3.2-3B-Instruct	BF16	-	64.43	78.01	73.42	70.09	71.49	–
	NVFP4	I	61.02	71.04	70.90	66.77	67.43	94.33
		H	59.91	64.82	69.77	65.59	65.02	90.95
		WUSH	61.25	71.78	71.08	67.18	67.82	94.87
	MXFP4	I	56.81	60.80	67.30	64.56	62.37	87.25
		H	55.99	61.11	68.36	64.09	62.39	87.27
		WUSH	58.45	68.60	69.99	66.54	65.89	92.17
Llama-3.1-8B-Instruct	BF16	-	72.76	85.06	80.01	77.90	78.93	–
	NVFP4	I	68.64	80.29	77.97	74.43	75.33	95.44
		H	66.96	77.41	77.29	74.35	74.00	93.75
		WUSH	68.83	78.57	78.22	75.47	75.28	95.37
	MXFP4	I	62.21	69.52	73.76	72.61	69.53	88.08
		H	63.03	75.44	75.51	71.90	71.47	90.54
		WUSH	66.85	75.16	77.28	73.56	73.21	92.75
Qwen3-8B	BF16	-	72.98	90.90	75.52	70.56	77.49	–
	NVFP4	I	70.47	88.40	74.44	69.53	75.71	97.70
		H	70.19	86.35	73.02	68.11	74.42	96.03
		WUSH	70.86	89.33	74.82	69.79	76.20	98.33
	MXFP4	I	67.69	84.23	71.24	67.40	72.64	93.74
		H	67.53	87.04	71.48	67.64	73.42	94.75
		WUSH	70.29	87.95	74.06	69.50	75.45	97.36
Qwen3-14B	BF16	-	77.18	91.96	79.84	74.27	80.81	–
	NVFP4	I	75.20	90.22	77.38	73.32	79.03	97.80
		H	74.98	92.04	77.76	72.38	79.29	98.12
		WUSH	75.43	91.78	78.82	73.18	79.80	98.75
	MXFP4	I	72.92	90.22	76.68	71.51	77.83	96.31
		H	73.13	87.41	76.29	71.67	77.13	95.44
		WUSH	74.56	91.87	78.18	73.15	79.44	98.30

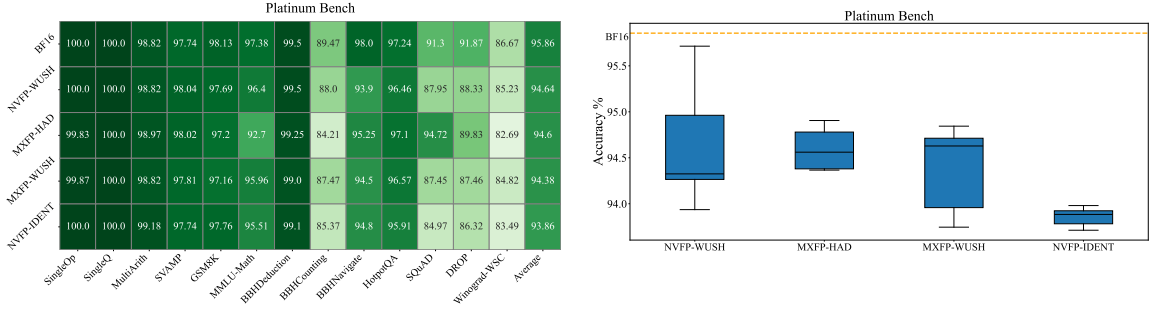


Figure 2: Comparison of different transforms on Qwen3-14B for both NVFP4 and MXFP4 RTN quantization on Platinum benchmark tasks. The left table shows accuracy results across the individual Platinum benchmark tasks, while the right plot shows the average accuracy scores together with their standard deviations for each transform.

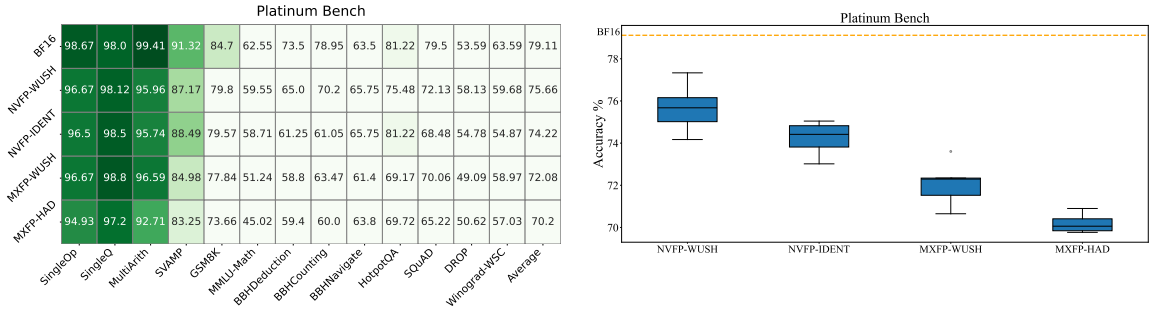


Figure 3: Comparison of different transforms on Llama3.2-3B Instruct for both NVFP4 and MXFP4 RTN quantization on Platinum benchmark tasks. The left table shows accuracy results across the individual Platinum benchmark tasks, while the right plot shows the average accuracy scores together with their standard deviations for each transform.

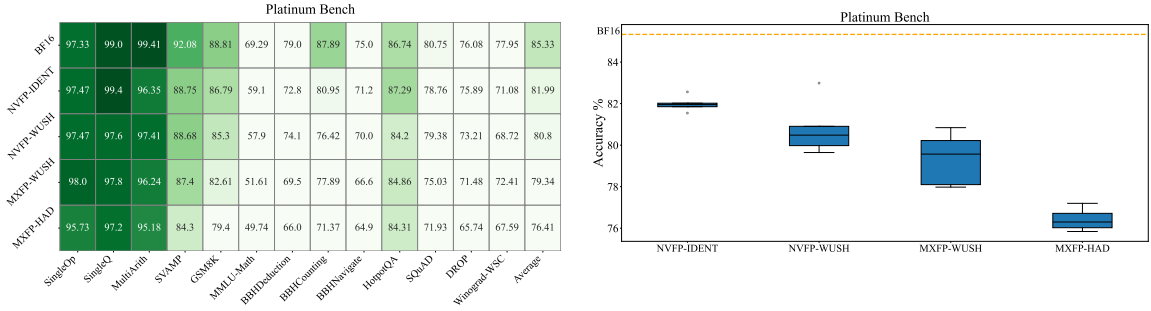


Figure 4: Comparison of different transforms on Llama3.1-8B Instruct for both NVFP4 and MXFP4 RTN quantization on Platinum benchmark tasks. The left table shows accuracy results across the individual Platinum benchmark tasks, while the right plot shows the average accuracy scores together with their standard deviations for each transform.

non-trivial and will require adapting both the optimization schedule and the calibration pipeline.

From a systems perspective, efficient kernel support for WUSH is another important direction. Unlike blockwise Hadamard rotations, which reuse a single transform across all blocks, WUSH generally assigns a distinct transform to each block. This per-block specialization complicates kernel reuse and fusion in existing low-level libraries.

Finally, it will be useful to explore structurally simplified variants of WUSH that trade optimality for lower computational overhead. One promising avenue is to approximate the data-aware component with a diagonal matrix, thereby reducing the cost of applying the transforms at inference time.

5 Conclusion

We have studied blockwise weight-activation quantization for LLMs in the presence of heavy-tailed outliers and have shown that, under mild assumptions, this problem admits closed-form linear transforms for both FP and INT block quantizers. Our construction, WUSH, combines a fixed Hadamard backbone with a data-aware component derived from second-order statistics, yielding a non-orthogonal blockwise transform that is provably optimal and remains amenable to efficient implementation. These results clarify the empirical success of Hadamard rotations and indicate that principled, data-aware block transforms can significantly narrow the gap between low-bit and full-precision models.

Acknowledgment

We would like to thank Tijmen Blankevoort for useful discussions and for suggesting the name WUSH, which is a clear improvement over our previous name (HSUW).

References

- Saleh Ashkboos, Iliia Markov, Elias Frantar, Tingxuan Zhong, Xincheng Wang, Jie Ren, Torsten Hoefer, and Dan Alistarh. QUIK: Towards end-to-end 4-bit inference on generative large language models. In Yaser Al-Onaizan, Mohit Bansal, and Yun-Nung Chen (eds.), *Proceedings of the 2024 Conference on Empirical Methods in Natural Language Processing*, pp. 3355–3371, Miami, Florida, USA, November 2024a. Association for Computational Linguistics. doi: 10.18653/v1/2024.emnlp-main.197. URL <https://aclanthology.org/2024.emnlp-main.197/>. 2
- Saleh Ashkboos, Amirkeivan Mohtashami, Maximilian L. Croci, Bo Li, Pashmina Cameron, Martin Jaggi, Dan Alistarh, Torsten Hoefer, and James Hensman. Quarot: Outlier-free 4-bit inference in rotated llms. In A. Globerson, L. Mackey, D. Belgrave, A. Fan, U. Paquet, J. Tomczak, and C. Zhang (eds.), *Advances in Neural Information Processing Systems*, volume 37, pp. 100213–100240. Curran Associates, Inc., 2024b. doi: 10.52202/079017-3180. URL https://proceedings.neurips.cc/paper_files/paper/2024/file/b5b939436789f76f08b9d0da5e81af7c-Paper-Conference.pdf. 1, 2, 3

- Jerry Chee, Yaohui Cai, Volodymyr Kuleshov, and Christopher M De Sa. Quip: 2-bit quantization of large language models with guarantees. In A. Oh, T. Naumann, A. Globerson, K. Saenko, M. Hardt, and S. Levine (eds.), *Advances in Neural Information Processing Systems*, volume 36, pp. 4396–4429. Curran Associates, Inc., 2023. URL https://proceedings.neurips.cc/paper_files/paper/2023/file/0df38cd13520747e1e64e5b123a78ef8-Paper-Conference.pdf. 2, 3
- Jiale Chen, Yalda Shabanzadeh, Elvir Crnčević, Torsten Hoefer, and Dan Alistarh. The geometry of llm quantization: Gptq as babai’s nearest plane algorithm, 2025. URL <https://arxiv.org/abs/2507.18553>. 2
- Alexandre Défossez, Yossi Adi, and Gabriel Synnaeve. Differentiable model compression via pseudo quantization noise. *Transactions on Machine Learning Research*, 2022. ISSN 2835-8856. URL <https://openreview.net/forum?id=DijnKziche>. 9
- Tim Dettmers, Mike Lewis, Younes Belkada, and Luke Zettlemoyer. Gpt3.int8(): 8-bit matrix multiplication for transformers at scale. In S. Koyejo, S. Mohamed, A. Agarwal, D. Belgrave, K. Cho, and A. Oh (eds.), *Advances in Neural Information Processing Systems*, volume 35, pp. 30318–30332. Curran Associates, Inc., 2022. URL https://proceedings.neurips.cc/paper_files/paper/2022/file/c3ba4962c05c49636d4c6206a97e9c8a-Paper-Conference.pdf. 1, 2
- Tim Dettmers, Ruslan A. Svirschevski, Vage Egiazarian, Denis Kuznedelev, Elias Frantar, Saleh Ashkboos, Alexander Borzunov, Torsten Hoefer, and Dan Alistarh. SpQR: A sparse-quantized representation for near-lossless LLM weight compression. In *The Twelfth International Conference on Learning Representations*, 2024. URL <https://openreview.net/forum?id=Q1u25ahSuy>. 2
- Vage Egiazarian, Roberto L. Castro, Denis Kuznedelev, Andrei Panferov, Eldar Kurtic, Shubhra Pandit, Alexandre Marques, Mark Kurtz, Saleh Ashkboos, Torsten Hoefer, and Dan Alistarh. Bridging the gap between promise and performance for microscaling fp4 quantization, 2025. URL <https://arxiv.org/abs/2509.23202>. 2, 3
- Elias Frantar and Dan Alistarh. Optimal brain compression: A framework for accurate post-training quantization and pruning. In S. Koyejo, S. Mohamed, A. Agarwal, D. Belgrave, K. Cho, and A. Oh (eds.), *Advances in Neural Information Processing Systems*, volume 35, pp. 4475–4488. Curran Associates, Inc., 2022. URL https://proceedings.neurips.cc/paper_files/paper/2022/file/1caf09c9f4e6b0150b06a07e77f2710c-Paper-Conference.pdf. 2
- Elias Frantar, Saleh Ashkboos, Torsten Hoefer, and Dan Alistarh. OPTQ: Accurate quantization for generative pre-trained transformers. In *The Eleventh International Conference on Learning Representations*, 2023. URL <https://openreview.net/forum?id=tcbBPnfwxS>. 1, 2
- Leo Gao, Jonathan Tow, Stella Biderman, Sid Black, Anthony DiPofi, Charles Foster, Laurence Golding, Jeffrey Hsu, Kyle McDonell, Niklas Muennighoff, et al. A framework for few-shot language model evaluation. *Zenodo*, 2021. 13

- Herve Jegou, Matthijs Douze, and Cordelia Schmid. Hamming embedding and weak geometric consistency for large scale image search. In *European conference on computer vision*, pp. 304–317. Springer, 2008. 2
- Herve Jegou, Matthijs Douze, and Cordelia Schmid. Product quantization for nearest neighbor search. *IEEE transactions on pattern analysis and machine intelligence*, 33(1): 117–128, 2010. 2
- Eldar Kurtic, Alexandre Noll Marques, Shubhra Pandit, Mark Kurtz, and Dan Alistarh. “give me bf16 or give me death”? accuracy-performance trade-offs in llm quantization. In *Proceedings of the 63rd Annual Meeting of the Association for Computational Linguistics (Volume 1: Long Papers)*, pp. 26872–26886, 2025. 1
- Ji Lin, Jiaming Tang, Haotian Tang, Shang Yang, Wei-Ming Chen, Wei-Chen Wang, Guangxuan Xiao, Xingyu Dang, Chuang Gan, and Song Han. Awq: Activation-aware weight quantization for on-device llm compression and acceleration. In P. Gibbons, G. Pekhimenko, and C. De Sa (eds.), *Proceedings of Machine Learning and Systems*, volume 6, pp. 87–100, 2024. URL https://proceedings.mlsys.org/paper_files/paper/2024/file/42a452cbafa9dd64e9ba4aa95cc1ef21-Paper-Conference.pdf. 1, 3
- Zechun Liu, Changsheng Zhao, Igor Fedorov, Bilge Soran, Dhruv Choudhary, Raghuraman Krishnamoorthi, Vikas Chandra, Yuandong Tian, and Tijmen Blankevoort. Spinqant: LLM quantization with learned rotations. In *The Thirteenth International Conference on Learning Representations*, 2025. URL <https://openreview.net/forum?id=og06DGE6FZ>. 2, 3
- Open Compute Project Foundation MX Alliance. OCP Microscaling Formats (MX) Specification Version 1.0. Technical specification, Open Compute Project Foundation, September 2023. URL <https://www.opencompute.org/documents/ocp-microscaling-formats-mx-v1-0-spec-final-pdf>. 3
- NVIDIA. Nvidia blackwell architecture technical brief. Technical report, NVIDIA, 2024. URL <https://resources.nvidia.com/en-us-blackwell-architecture>. 3
- Guilherme Penedo, Hynek Kydlíček, Loubna Ben allal, Anton Lozhkov, Margaret Mitchell, Colin Raffel, Leandro Von Werra, and Thomas Wolf. The fineweb datasets: Decanting the web for the finest text data at scale. In A. Globerson, L. Mackey, D. Belgrave, A. Fan, U. Paquet, J. Tomczak, and C. Zhang (eds.), *Advances in Neural Information Processing Systems*, volume 37, pp. 30811–30849. Curran Associates, Inc., 2024. doi: 10.52202/079017-0970. URL https://proceedings.neurips.cc/paper_files/paper/2024/file/370df50ccfd8bde18f8f9c2d9151bda-Paper-Datasets_and_Benchmarks_Track.pdf. 12
- Yuantian Shao, Peisong Wang, Yuanteng Chen, Chang Xu, Zhihui Wei, and Jian Cheng. Block rotation is all you need for mxfp4 quantization, 2025. URL <https://arxiv.org/abs/2511.04214>. 3

- Yuxuan Sun, Ruikang Liu, Haoli Bai, Han Bao, Kang Zhao, Yuening Li, Jiaxin Hu, Xianzhi Yu, Lu Hou, Chun Yuan, et al. Flatquant: Flatness matters for llm quantization. *arXiv preprint arXiv:2410.09426*, 2024. 2
- Albert Tseng, Jerry Chee, Qingyao Sun, Volodymyr Kuleshov, and Christopher De Sa. QuIP#: Even better LLM quantization with hadamard incoherence and lattice codebooks. In Ruslan Salakhutdinov, Zico Kolter, Katherine Heller, Adrian Weller, Nuria Oliver, Jonathan Scarlett, and Felix Berkenkamp (eds.), *Proceedings of the 41st International Conference on Machine Learning*, volume 235 of *Proceedings of Machine Learning Research*, pp. 48630–48656. PMLR, 21–27 Jul 2024a. URL <https://proceedings.mlr.press/v235/tseng24a.html>. 2, 3
- Albert Tseng, Qingyao Sun, David Hou, and Christopher De. Qtip: Quantization with trellises and incoherence processing. In A. Globerson, L. Mackey, D. Belgrave, A. Fan, U. Paquet, J. Tomczak, and C. Zhang (eds.), *Advances in Neural Information Processing Systems*, volume 37, pp. 59597–59620. Curran Associates, Inc., 2024b. doi: 10.52202/079017-1904. URL https://proceedings.neurips.cc/paper_files/paper/2024/file/6de2e84b8da47bb2eb5e2ac96c63d2b0-Paper-Conference.pdf. 3
- Joshua Vendrow, Edward Vendrow, Sara Beery, and Aleksander Madry. Do large language model benchmarks test reliability? *arXiv preprint arXiv:2502.03461*, 2025. 13
- Guangxuan Xiao, Ji Lin, Mickael Seznec, Hao Wu, Julien Demouth, and Song Han. SmoothQuant: Accurate and efficient post-training quantization for large language models. In Andreas Krause, Emma Brunskill, Kyunghyun Cho, Barbara Engelhardt, Sivan Sabato, and Jonathan Scarlett (eds.), *Proceedings of the 40th International Conference on Machine Learning*, volume 202 of *Proceedings of Machine Learning Research*, pp. 38087–38099. PMLR, 23–29 Jul 2023. URL <https://proceedings.mlr.press/v202/xiao23c.html>. 1, 3

Appendix A. Maximum Inequalities for Tail-Bounded Distributions

Lemma 5 (Expectation from the Survival Function) *Let $X \geq 0$ be a random variable with the density function f and the survival function $S(t) = \mathbb{P}(X \geq t)$ with $t \geq 0$. Let $g : [0, \infty) \rightarrow \mathbb{R}$ be integrable and define $G(t) = \int_0^t g(u) du$. Assume that $\lim_{t \rightarrow \infty} G(t) S(t) = 0$. Then $\mathbb{E}G(X) = \int_0^\infty g(t) S(t) dt$.*

Proof Since X has density f and takes values in $[0, \infty)$, $\mathbb{E}G(X) = \int_0^\infty G(t) f(t) dt$. The survival function satisfies $S(t) = \mathbb{P}(X \geq t) = \int_t^\infty f(u) du$, so S is differentiable almost everywhere with $S'(t) = -f(t)$. Hence, $\mathbb{E}G(X) = \int_0^\infty G(t) f(t) dt = -\int_0^\infty G(t) S'(t) dt$. We now integrate by parts, using $G'(t) = g(t)$,

$$-\int_0^\infty G(t) S'(t) dt = -[G(t) S(t)]_0^\infty + \int_0^\infty g(t) S(t) dt. \quad (26)$$

By definition, $G(0) = 0$, and by assumption $\lim_{t \rightarrow \infty} G(t) S(t) = 0$, the boundary term $[G(t) S(t)]_0^\infty = 0$. Therefore, $\mathbb{E}G(X) = \int_0^\infty g(t) S(t) dt$. \blacksquare

A.1 Gaussian Distribution

Definition of sub-Gaussian.

A probability distribution of a random variable $X \in \mathbb{R}$ is called sub-Gaussian with variance proxy σ^2 if $\mathbb{E} \exp((X - \mathbb{E}X)t) \leq \exp(2^{-1}\sigma^2 t^2)$ for all $t \in \mathbb{R}$, and the smallest such σ^2 is called the optimal variance proxy.

Basic properties of sub-Gaussian distributions.

The variance proxy is larger than or equal to the variance: $\sigma^2 \geq \mathbb{E}(X - \mathbb{E}X)^2$. For a Gaussian distribution, the optimal variance proxy is the same as the variance.

Chernoff bound on the tail: $\mathbb{P}(|X - \mathbb{E}X| \geq t) \leq 2 \exp(-2^{-1}\sigma^2 t^2)$ for all $t \geq 0$.

Maximum inequality.

Let X_1, \dots, X_d be zero-mean Gaussian random variables with variance $\sigma_1^2, \dots, \sigma_d^2$. Denote $\sigma_\star^2 = \max_k \sigma_k^2 = \max_k \mathbb{E}X_k^2$ as the smallest variance proxy for X_1, \dots, X_d . Using Lemma 5,

$$\begin{aligned} \mathbb{E} \max_k X_k^2 &= 2 \int_0^\infty t \mathbb{P}\left(\max_k |X_k| \geq t\right) dt = 2 \int_0^\infty t \mathbb{P}\left(\bigcup_{k=1}^d \{|X_k| \geq t\}\right) dt \\ &\leq 2 \int_0^{t_\star} t \, 1 \, dt + 2 \int_{t_\star}^\infty t \left(\sum_{k=1}^d \mathbb{P}(|X_k| \geq t)\right) dt \\ &\leq 2 \int_0^{t_\star} t \, dt + 2d \int_{t_\star}^\infty t \left(\max_k \mathbb{P}(|X_k| \geq t)\right) dt \\ &\leq 2 \int_0^{t_\star} t \, dt + 4d \int_{t_\star}^\infty t \exp(-2^{-1}\sigma_\star^{-2}t^2) dt = [t^2]_0^{t_\star} + 4d [-\sigma_\star^2 \exp(-2^{-1}\sigma_\star^{-2}t^2)]_{t_\star}^\infty \\ &= t_\star^2 + 4d\sigma_\star^2 \exp(-2^{-1}\sigma_\star^{-2}t_\star^2). \end{aligned} \quad (27)$$

Splitting at $t_\star = \sigma_\star \sqrt{2 \ln(2d)}$ gives

$$\mathbb{E} \max_k X_k^2 \leq 2\sigma_\star^2 \ln(2d) + 2\sigma_\star^2 = (2 \ln(2d) + 2) \max_k \mathbb{E} X_k^2 \quad (28)$$

without needing the independence of X_k . Also, considering the trivial bound $\mathbb{E} \max_k X_k^2 \leq \mathbb{E} \sum_{k=1}^d X_k^2 = \sum_{k=1}^d \mathbb{E} X_k^2 \leq d \max_k \mathbb{E} X_k^2$, then $\mathbb{E} \max_k X_k^2 \leq \min\{d, (2 \ln(2d) + 2)\} \max_k \mathbb{E} X_k^2$.

A.2 Laplacian Distribution

For a random variable $X \sim \text{Laplace}(\mu, b)$ and $t \geq 0$,

$$\mathbb{P}(|X - \mu| \geq t) = 2 \int_t^\infty 2^{-1} b^{-1} \exp(-b^{-1}x) dx = \exp(-b^{-1}t). \quad (29)$$

The variance $\mathbb{E}(X - \mathbb{E}X)^2 = 2b^2$.

Let X_1, \dots, X_d be zero-mean Laplacian random variables with diversity b_1, \dots, b_d . Denote $b_\star = \max_k b_k = \sqrt{\frac{1}{2} \max_k \mathbb{E} X_k^2}$. For $t \geq 0$, $\mathbb{P}(|X_k| \geq t) = \exp(-b_k^{-1}t) \leq \exp(-b_\star^{-1}t)$. Using Lemma 5,

$$\begin{aligned} \mathbb{E} \max_k X_k^2 &= 2 \int_0^\infty t \mathbb{P}\left(\max_k |X_k| \geq t\right) dt = 2 \int_0^\infty t \mathbb{P}\left(\bigcup_{k=1}^d \{|X_k| \geq t\}\right) dt \\ &\leq 2 \int_0^{t_\star} t \, 1 \, dt + 2 \int_{t_\star}^\infty t \left(\sum_{k=1}^d \mathbb{P}(|X_k| \geq t)\right) dt \\ &\leq 2 \int_0^{t_\star} t \, dt + 2d \int_{t_\star}^\infty t \left(\max_k \mathbb{P}(|X_k| \geq t)\right) dt \\ &\leq 2 \int_0^{t_\star} t \, dt + 2d \int_{t_\star}^\infty t \exp(-b_\star^{-1}t) dt = [t^2]_0^{t_\star} + 2d [-b_\star(t + b_\star) \exp(-b_\star^{-1}t)]_{t_\star}^\infty \\ &= t_\star^2 + 2db_\star(t_\star + b_\star) \exp(-b_\star^{-1}t_\star). \end{aligned} \quad (30)$$

Splitting at $t_\star = b \ln d$ gives

$$\mathbb{E} \max_k X_k^2 \leq b_\star^2 \left((\ln d)^2 + 2 \ln d + 2\right) = \left(2^{-1} (\ln d)^2 + \ln d + 1\right) \max_k \mathbb{E} X_k^2 \quad (31)$$

without needing the independence of X_k .